JOURNAL OF MATERIALS SCIENCE 27 (1992) 2922–2933

Low temperature synthesis of $CaO–SiO_2$ glasses having stable liquid–liquid immiscibility by the sol–gel process

N. P. BANSAL
National Aeronautics and Space Administration, Lewis Research Center, Cleveland, OH 44135, USA

Calcium silicate glass compositions lying within the liquid–liquid immiscibility dome of the phase diagram, which could not have been prepared by the conventional melting method, have been synthesized by the sol–gel process. Hydrolysis and polycondensation of tetraethyl orthosilicate (TEOS) solutions containing up to 20 mol% calcium nitrate, resulted in the formation of clear and transparent gels. The gel formation time decreased with increase in water:TEOS mole ratio, calcium content and the reaction temperature. Smaller values of gel times in the presence of calcium nitrate are probably caused by lowering of the ionic charge on the sol particles by the salt present. The gelation activation energy, E_{gel}, was evaluated from the temperature dependence of the gel time. Neither the presence of Ca^{2+} ions nor the water:TEOS mole ratio had any appreciable effect on the value of E_{gel}. The presence of glycerol in the solution helped in the formation of crack-free monolithic gel specimens. Chemical and structural changes occurring in the gels, as a function of the heat treatments, have been monitored using differential thermal analysis, thermogravimetric analysis, infrared spectroscopy, X-ray diffraction, surface-area and pore-size distribution measurements.

1. Introduction

Low-temperature synthesis of glass compositions lying within the liquid–liquid immiscibility region has been reported by a number of researchers [1–5]. Relatively, only a few such glasses containing alkaline earth metal oxides have been prepared by the sol–gel procedure; $CaO–SiO_2$ by Hayashi and Saito [2], $SrO–SiO_2$ by Yamane and Kojima [3], and $MgO–SiO_2$ by Bansal [1]. Preparation of gels in the $CaO–Al_2O_3–SiO_2$ system using tetraethoxysilane (TEOS), aluminium sec-butoxide, and calcium nitrate has been investigated by Pancrazi *et al.* [6]. Tredway and Risbud [7] used TEOS, aluminium sec-butoxide and barium acetate for the synthesis of $BaO–Al_2O_3–SiO_2$ gel. Earlier attempts [2] to prepare $CaO–SiO_2$ glasses by the gel method using calcium nitrate as the source of calcium oxide, resulted in white powders containing crystalline $Ca(NO_3)_2 \cdot nH_2O$ ($n = 0, 1, 2$). The possibility of introducing the modifier cation as an alcoholic solution of calcium nitrate into silicon tetraethoxide has been examined in the present investigation.

The objective of the present study was to synthesize $CaO–SiO_2$ glass compositions having liquid–liquid immiscibility, which cannot be prepared by the conventional melting technique, using the sol–gel process. These compositionally homogeneous precursor materials were also needed to study the effects of microgravity on liquid–liquid phase separation in glasses.

Gels of various compositions lying within the liquid–liquid immiscibility dome of the $CaO–SiO_2$ system were synthesized under different experimental conditions using TEOS and calcium nitrate as the starting materials. Structural developments in the gels as a function of the thermal treatment were monitored using several techniques. The results of these investigations are presented in this paper.

2. Experimental procedure

2.1. Materials

Tetraethyl orthosilicate (TEOS), calcium nitrate tetrahydrate (analytical reagent), and 200 proof absolute ethyl alcohol were used as-received. Calcium alkoxides are only slightly soluble in common solvents. The solubilities [8] of calcium methoxide and calcium ethoxide in their parent alcohol are only 2.3 and 75 mmol l^{-1}, respectively. When suitable alkoxide is not available, the acetate or nitrate salt of the metal is used. Calcium acetate is soluble in water but almost insoluble in alcohol. Calcium nitrate is soluble both in water and alcohol. An alcoholic solution of calcium nitrate was consequently used as the source of calcium.

2.2. Gel synthesis

The method of gel synthesis was similar to that described earlier [1, 9]. A flow diagram of the procedure

0022–2461

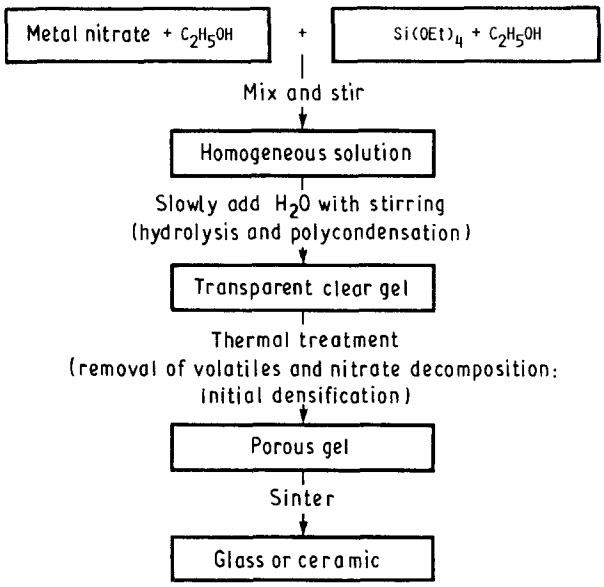

Figure 1 Flow chart of glass synthesis by the sol–gel method.

used for glass preparation by the sol–gel process is shown in Fig. 1. An alcoholic solution of calcium nitrate tetrahydrate was mixed under continuous stirring with TEOS which had been diluted with ethanol. The calculated amount of water was then slowly added dropwise under vigorous stirring resulting in a homogeneous clear solution. The container was sealed with parafilm and left to stand for gelation under ambient conditions or in a constant temperature bath. The pH of some solutions was monitored as a function of time using a Fisher Accumet (Model 815 MP) pH meter. The gel formation was complete, as tested by tilting the container, in less than an hour to several days, depending upon the reaction temperature, water concentration, and the calcium content. Clear and transparent bulk gels were obtained which cracked into smaller pieces on slow drying under ambient conditions. To prepare monolithic gel samples, ~ 2 wt % glycerol was added to the solution as the drying control agent. The gels were stored at room temperature for several days followed by drying and calcination at higher temperatures.

2.3. Characterization of gels

Chemical and structural evolution of gels as a function of the heat treatment was followed using a number of techniques. Differential thermal analysis (DTA) and thermogravimetric analysis (TGA) were carried out using Perkin-Elmer DTA-1700 and TGS-2 systems, respectively, which were interfaced with computerized data acquisition and analysis systems. A Netzsch thermal analyser STA-429 with a super kanthal heating element furnace was also used for simultaneous recording of DTA and TGA on the same specimen. Infrared transmission spectra were recorded from 400–4000 cm^{-1} using the KBr pellet method with a Perkin–Elmer 1750 Fourier transform infrared spectrometer interfaced with a Perkin–Elmer 7300 professional computer. X-ray powder diffraction patterns were recorded at room temperature using a step scan procedure (0.03°/2θ step, count time 0.4 s) on a Phillips ADP-3600 automated powder diffractometer equipped with a crystal monochromator employing CuK_α radiation. BET surface area and pore volume measurements were made from the nitrogen adsorption isotherms at 77 K using Micromeritics Digisorb 2500 system. Krypton gas adsorption was used for some specimens having a low surface area. Fractured surfaces of the sintered gel samples were examined using a Cambridge Stereoscan 200 scanning electron microscope (SEM). A thin layer of gold was evaporated on to the sample surface before viewing in the SEM.

3. Results

3.1. Gel formation

Chemical compositions of the glasses synthesized and their acronyms are given in Table I. All the compositions lie within the liquid–liquid immiscibility region of the CaO–SiO_2 phase diagram as shown in Fig. 2.

Monolithic gel specimens of 10CS composition were prepared in the presence of glycerol as the drying control agent. On slow drying for several weeks under ambient conditions, the gel samples typically reduced to about one-tenth of the original volume as shown in Fig. 3. A typical crack-free monolithic body is shown in the foreground of Fig. 3.

The gelation times and gel appearance under ambient conditions for solutions of various compositions are given in Table II. All the gels were clear and gel formation time decreased with increase in calcium concentration. However, the value of water: TEOS mole ratio, r, was not the same for different solutions.

Typical values of solution pH as a function of time for four different compositions for $r = 6$ at room temperature are given in Table III. There is a systematic decrease in pH with increase in Ca^{2+} concentration. The pH of the solution with no calcium drops from 5.8 to 5.06 after 24 h. In contrast, the solutions containing Ca^{2+} show hardly any change in pH after ~ 24 h.

Fig. 4 shows the influence of water:TEOS mole ratio on time of gel formation for the $10CaO$–$90SiO_2$ composition at room temperature. The values of gelation time for $10CaO$–$90SiO_2$ composition for $r = 4$, 6, and 7.5 at various temperatures are listed in Table IV. For comparison the data for TEOS for $r = 6$ are also given. The value of t_{gel} decreases with increase in r or temperature. Also, the presence of Ca^{2+} greatly lowers the time taken for gel formation in comparison to TEOS.

TABLE I Acronyms for the glass compositions studied

Acronym	Mol %		Wt %	
	CaO	SiO_2	CaO	SiO_2
2CS	2	98	1.87	98.13
5CS	5	95	4.68	95.32
10CS	10	90	9.38	90.62
15CS	15	85	14.12	85.88
20CS	20	80	18.89	81.11

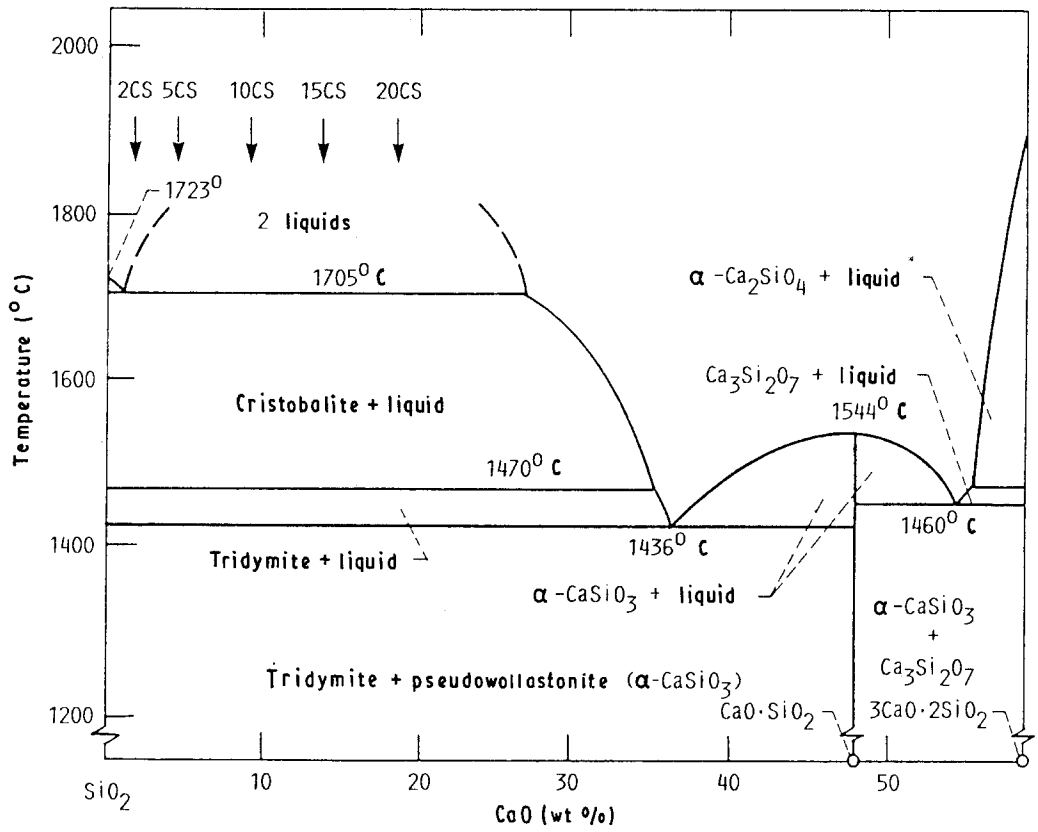

Figure 2 Partial phase diagram of $CaO–SiO_2$ system showing positions of the various glass compositions investigated.

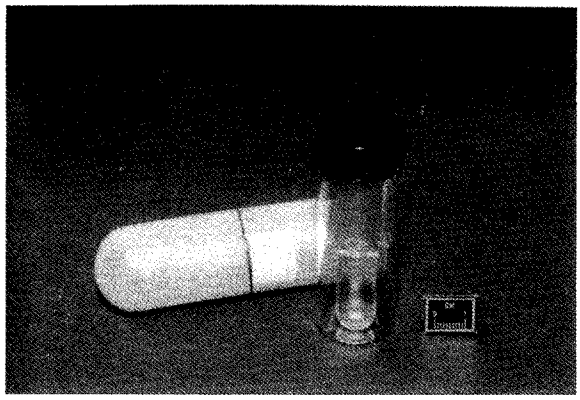

Figure 3 Monolithic $10CaO–90SiO_2$ (mol %) gel specimen, prepared using glycerol as the drying control chemical additive, and after drying for several weeks under ambient conditions (foreground).

Table V shows the effect of Ca^{2+} ion concentration in the solution on gelation times at various temperatures for $r = 6$. By the addition of just 2 mol % Ca^{2+}, gelation time is greatly reduced. At any temperature, the time of gelation decreases with increase in Ca^{2+} ion concentration. The effect is more pronounced at low concentration and seems to level off at higher concentrations of the metal ion. The reduction in gelling time in the presence of Ca^{2+} ions may be due to the lowering of ionic charge on sol particles by the salt.

3.2. Thermal analysis

DTA thermograms of gels of different compositions, which had been dried for several weeks at room temperature, were recorded at a heating rate of 5 °C min^{-1} in air. Typical DTA curves for the 2CS and 20CS compositions are shown in Fig. 5. The broad endothermic peak at 120 °C for 2CS and at 130 °C for 20CS gel may be attributed to the evaporation of physically adsorbed water and alcohol. The sharp endothermic peak for 2CS at 215 °C and two sharp endotherms for 20CS at 188 and 237 °C may be assigned to the volatilization of organic species such as ethers and esters which might have formed as a result of the reactions taking place during the sol–gel process. The broad exothermic peak at 398 °C for 2CS and at 387 °C for 20CS may be ascribed to the pyrolysis of the residual organic groups and the decomposition of nitrate. Brown fumes, probably of NO_2, were observed during pyrolysis of the gels at ~ 400–500 °C.

TGA and DTGA curves of various room-temperature dried gels were also recorded under air flow at a heating rate of 5 °C min^{-1}. Typical curves for the 2CS and 20CS gels are presented in Fig. 6. The temperatures corresponding to various weight losses in the TGA are in excellent agreement with the DTA results. Gradual weight loss above ~ 600 °C may be assigned to the network condensation. Total weight loss from the 20CS gel sample (38.3 %) is much higher than from 2CS (~ 22.1%) due to the higher nitrate content in the former.

3.3. Pyrolysis of gels

Gels of various compositions were allowed to stand under ambient conditions for several months followed by drying for a week at ~ 66 °C in air. The resulting

TABLE II Batch compositions, gelation time, and gel appearance at ambient temperature for $CaO–SiO_2$ system[a]

System	$Ca(NO_3)_2 \cdot 4H_2O$ (g)	H_2O:$Si(OC_2H_5)_4$ (mole ratio)	Gelation time (h)	Gel appearance
2CS	1.16	4.59	73	Clear
5CS	2.99	4.72	55	Clear
10CS	6.31	4.96	43.5	Clear
15CS	10.02	5.22	36	Clear
20CS	14.19	5.52	31	Clear

[a] 50 g $Si(OC_2H_5)_4$, and 80 ml C_2H_5OH.

TABLE III pH of various solutions as a function of time at room temperature; water:TEOS mole ratio = 6, TEOS = 50 g, C_2H_5OH = 80 ml

SiO_2		$2CaO–98SiO_2$[a]		$5CaO–95SiO_2$		$10CaO–90SiO_2$	
Reaction time	pH	Reaction time	pH	Reaction time	pH	Reaction time	pH
3 min	5.80	5 min	4.26	5 min	4.18	5 min	4.00
5 min	5.43	15 min	4.30	15 min	4.18	15 min	4.00
10 min	5.38	30 min	4.30	30 min	4.19	30 min	3.98
35 min	5.26	40 min	4.30	2 h	4.14	1 h	3.96
50 min	5.26	1.5 h	4.25	5 h	4.12	3 h	3.96
1.5 h	5.29	3 h	4.26	6 h	4.12	20 h	3.95
2.5 h	4.51	21 h	4.23	24 h	4.14		
5.0 h	4.77						
7.0 h	4.92						
24 h	5.06						

[a] All compositions in mol %.

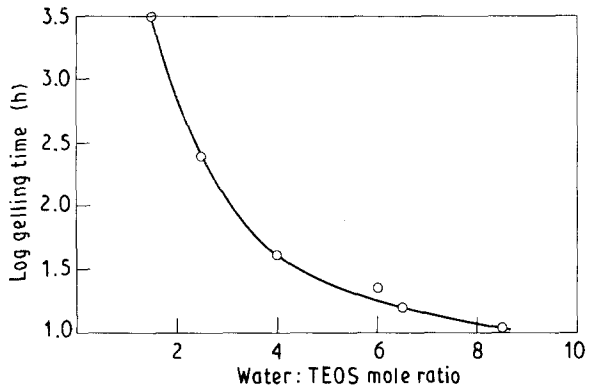

Figure 4 Effect of water:TEOS mole ratio on gelling time of $10CaO–90SiO_2$ (mol %) composition at room temperature. $Si(OC_2H_5)_4$ = 50 g, C_2H_5OH = 80 ml, and $Ca(NO_3)_2 \cdot 4H_2O$ = 6.31 g.

gels were transparent, colourless, and amorphous. These were then calcined under dynamic air flow at a heating rate of $\sim 2\,^{\circ}C\,min^{-1}$ to different temperatures (2CS, 5CS, and 10CS to 800 °C, 15CS to 780 °C, and 20CS to 740 °C) and furnace cooled. After this heat treatment all the samples remained colourless, glassy, and transparent except for the 15CS and 20CS which had turned white. The 10CS composition was further treated in air for 23 h at 800 °C when it turned white and opaque, at 900 °C for 8 h, and at 1000 °C for 5 h.

Another part of the 10CS gel was subjected to isothermal heat treatments for 24 h each at 100, 300, 500, 600, and 700 °C, followed by 17 h at 780 °C and 16 h at 860 °C in air. Part of the sample was saved for characterization after pyrolysis at each temperature. The gel became light yellow in colour after the 100 °C heat treatment. The yellow colour disappeared when the gel was fired at 300 °C. The sample had turned into white powder after the 700 °C calcination and remained so following the subsequent heat treatments at higher temperatures.

3.4. Infrared spectroscopy

Infrared absorption spectra in the 400–4000 cm^{-1} range for the 10CS gel dried for several weeks under ambient conditions is shown in Fig. 7. Fig. 8 compares the infrared spectra of 10CS gel calcined in air at various temperatures. The heat treatments are cumulative at subsequent temperatures. Infrared spectra of gels of different compositions heated to 740–800 °C in flowing air at $\sim 2\,^{\circ}C\,min^{-1}$ and furnace cooled are presented in Fig. 9. Positions of various infrared absorption peaks observed and their assignments [10–19] are shown in Fig. 7 and also listed in Table VI. The absorption peak around 950 cm^{-1}, attributed to the Si–O terminal non-bridging vibration, decreased in intensity with increasing firing temperature indicating the decrease of non-bridging oxygens. It is present only as a shoulder in the 300 °C heated sample and has completely disappeared in the 500 °C heated specimen indicating slow polymerization of residual Si–OH bonds at these temperatures. The strongest absorption peak at $\sim 1080\ cm^{-1}$, ascribed to Si–O–Si stretching vibration in SiO_4 tetrahedra, shows a slight shift to higher frequencies with increase in calcination temperature suggesting the strengthening of the Si–O

TABLE IV Influence of water:TEOS mole ratio on gelation of SiO_2 and $10CaO–90SiO_2$ systems at various temperatures

System	H_2O:TEOS mole ratio	Gelling time (h) at temp. (°C)					Arrhenius parameters	
		2	23	40.5	58	68	E^* (kJ mol^{-1})	A' (s^{-1})
SiO_2	6	–	156	38.5	15.3	7.9	54.5	7.8×10^3
10CS	4	–	40[a]	12	4.3[c]	2.4	52.9	1.5×10^4
	6	–	23[b]	7.5	2.5	1.3	55.8	7.4×10^4
	7.5	130	23.5	6	2.1	1.1[d]	56.9	1.3×10^5

[a] At 23.5 °C.
[b] At 25 °C.
[c] At 57.5 °C.
[d] At 67 °C.

TABLE V Influence of Ca^{2+} concentration on gelation of TEOS at various temperatures; water:TEOS mole ratio = 6

System (mol %)	Gelling time (h) at temperature (°C)					Arrhenius parameters	
	1	23	40.5	58	68	E^* (kJ mol^{-1})	A' (s^{-1})
SiO_2	–	156	38.5	15.3	7.9	54.5	7.8×10^3
$2CaO–98SiO_2$	260	44	10.3	4	2.6[b]	54.7	3.0×10^4
$5CaO–95SiO_2$	–	27[a]	8.5	3	1.6	55.2	4.9×10^4
$10CaO–90SiO_2$	–	23[a]	7.5	2.5	1.3	55.8	7.3×10^4

[a] At 25 °C.
[b] At 67 °C.

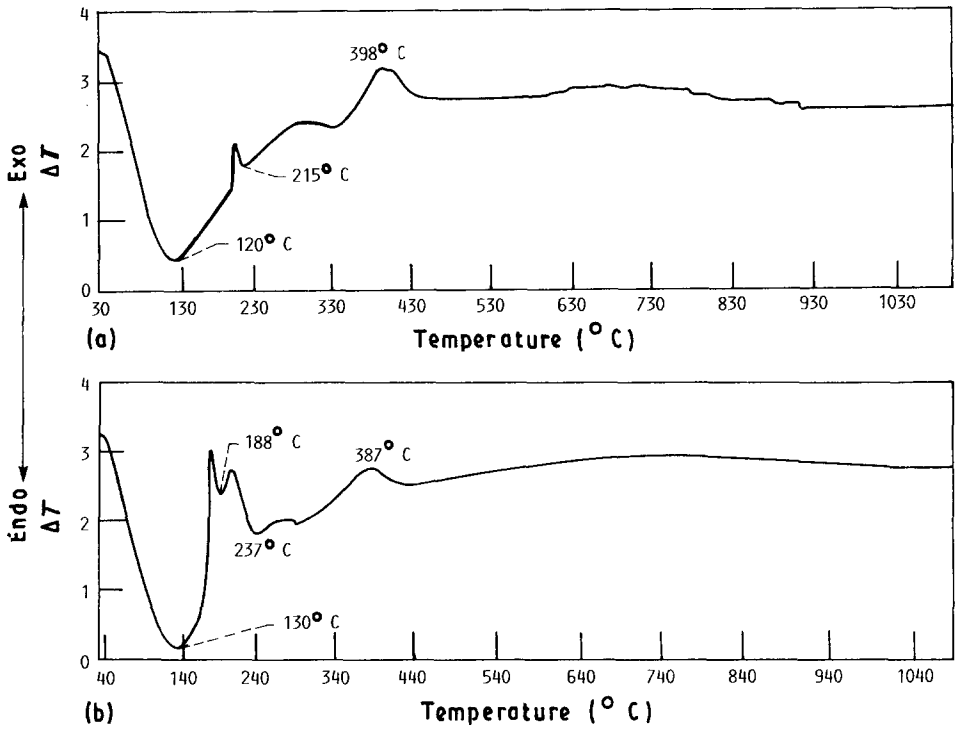

Figure 5 DTA scans of (a) 2CS, and (b) 20CS gels after drying for several weeks under ambient conditions; heating rate 5 °C min^{-1} in flowing air.

bonds in the tetrahedra. A similar shift in this peak was also reported by Varshneya and Suh [20], and by Kamiya *et al.* [19]. However, no such shift was observed in the $MgO–SiO_2$ gels in an earlier study by the present author [1]. The bands around 460 and 800 cm^{-1} are assigned to bending modes of Si–O–Si and O–Si–O bonds, respectively. The intensity of the peak around 1385 cm^{-1}, attributed [17] to the $-NO_3$ group, increased with the calcium nitrate concentration in the gel, decreased with increase in heat-treatment temperature, and is completely absent in the 700 °C heated sample. A very weak 1385 cm^{-1} peak in the specimens fired for 24 h at 500 or 600 °C implies a very slow rate of nitrate decomposition at these temperatures. The broad absorption bands around 1640 and 3450 cm^{-1}, attributed to water absorption, decreased in intensity with increase in heat-treatment temperature. The broad high-frequency peak at

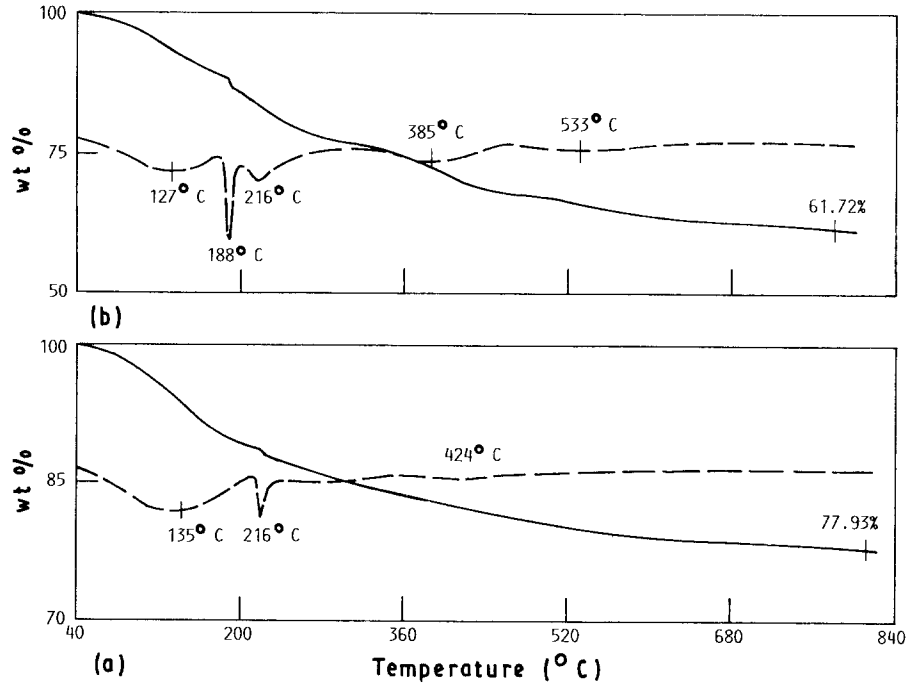

Figure 6 TGA and DTGA curves for (a) 2CS, and (b) 20CS gels after drying for several weeks under ambient conditions; scan rate 5 °C min^{-1} in flowing air.

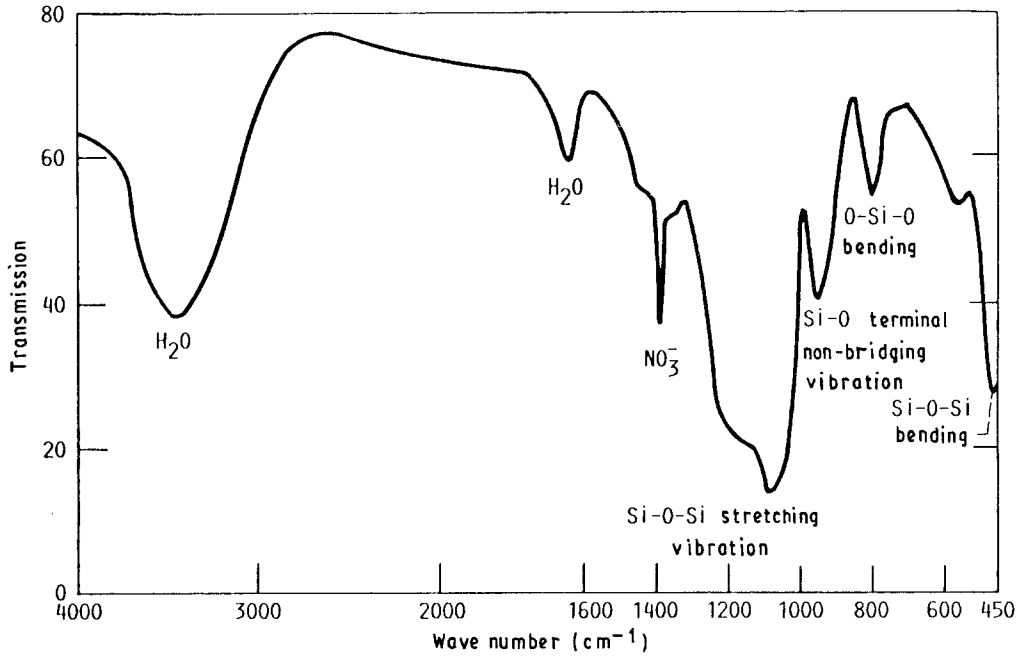

Figure 7 Infrared spectra of $10CaO–90SiO_2$ (mol %) gel after drying for several weeks under ambient conditions; water:TEOS mole ratio = 4.95.

$\sim 3450\ cm^{-1}$ is assigned to the superposition of physically absorbed water, hydrogen-bonded hydroxyl groups, and, at higher temperature, isolated –OH. Gel samples heat treated at temperatures as high as 800–860 °C still showed the presence of traces of water, but no absorption peaks attributable to organic groups were present. This may be due to the absorption of atmospheric moisture during the infrared sample preparation by mixing with undried KBr. The double peak around 2340 and 2360 cm^{-1}, attributed to absorption by the atmospheric CO_2, is present in some of the spectra.

3.5. X-ray diffraction

Structural changes occurring in the gels as a function of the thermal treatments were monitored by XRD. All the $CaO–SiO_2$ gels dried at ~ 66 °C for 7 days were amorphous to X-rays as shown in Fig. 10. These gels, when further calcined in air at ~ 2 °C min^{-1} to various temperatures and furnace cooled, were found to be amorphous by XRD (Fig. 11) except for the 2CS composition which showed the precipitation of small amounts of α-quartz. The 10CS composition was subjected to further isothermal heat treatments and the XRD spectra are given in Fig. 12. It was amorphous to

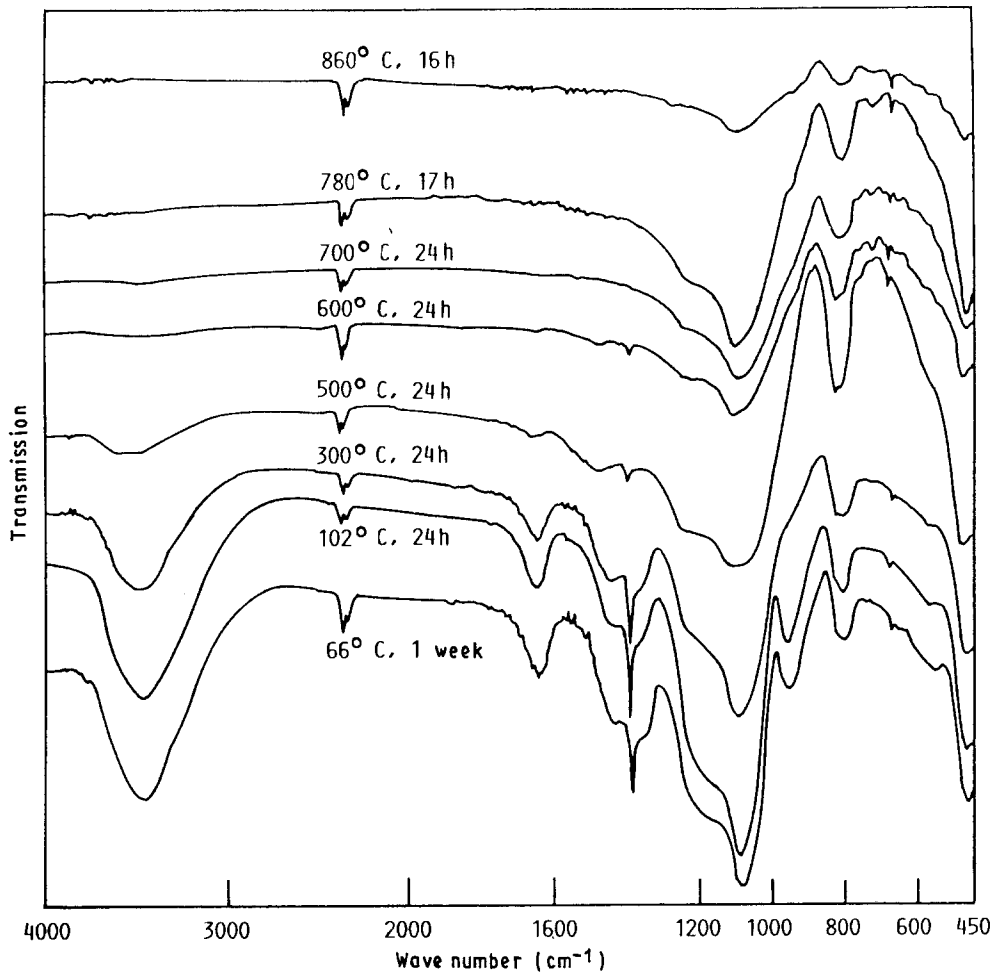

Figure 8 Infrared spectra of $10CaO–90SiO_2$ (mol %) gel calcined in air under different conditions. The heat treatments are cumulative at subsequent temperatures.

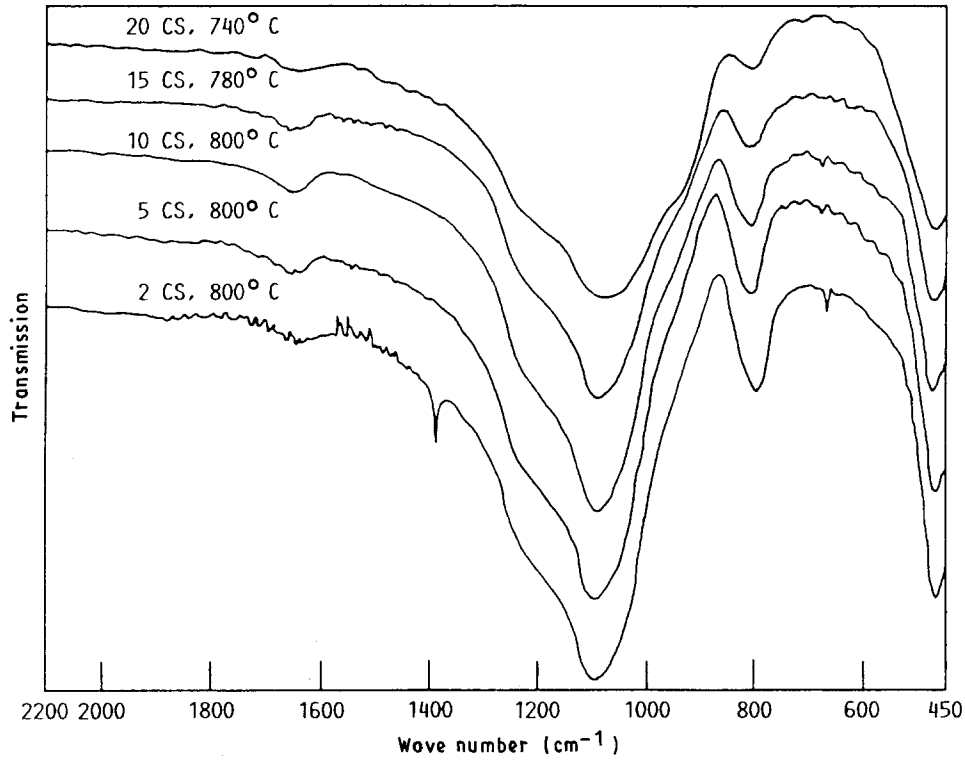

Figure 9 Infrared spectra of $CaO–SiO_2$ gels of various compositions heated to various temperatures at $\sim 2\,^{\circ}C\,min^{-1}$ in air and furnace cooled.

TABLE VI Infrared absorption peaks observed in $CaO–SiO_2$ gels and glasses and their assignments

Frequencies of infrared absorption bands (cm^{-1})	Functional group
460	Bending modes of Si–O–Si bonds
800	Bending modes of O–Si–O bonds
950	Si–OH bonds containing nonbridging oxygen
1080	Stretching vibration of Si–O–Si bonds
1385	$-NO_3$ group
1640	H_2O
3450	H_2O

X-rays after heat treatment at 800 °C for 23 h. However, low-intensity peaks of α-cristobalite were detected after firing for 8 h at 900 °C. On further calcination at 1000 °C for 5 h, α-cristobalite and the strongest peak of wollastonite ($CaSiO_3$) at $2\theta = 29.9°$ were present in the XRD. Hayashi and Saito [2] reported the precipitation of wollastonite ($CaSiO_3$) in $CaO–SiO_2$ gels when heated above 800 °C. Yamane and Kojima [3] attributed the decrease in transparency of $SrO–SiO_2$ gels, when heated to high temperatures, to the crystallization of α-quartz. The precipitation of α-quartz has also been observed by the present author [1] in $MgO–SiO_2$ gels when heated to ~ 950 °C. Precipitation of β-quartz has been reported [5] in gels of composition $4Na_2O–10.5B_2O_3–85.5SiO_2$ (mol %) when heated to 750 °C for 0.5 h. However, α-cristobalite was the crystalline phase when calcined at 750 °C for a longer time or for only 15 min at 800 °C or above.

The 10CS gel was also isothermally calcined at various temperatures starting from 102 °C for different times and the XRD patterns of the resulting specimens are shown in Fig. 13. The gel samples heat treated at 780 °C or above showed the presence of weak diffraction peaks in the XRD which could not be assigned to any known phase.

3.6. Surface area and pore size distribution

The pore volume and BET surface area calculated from the adsorption isotherms for the 10CS gel with $r = 4.95$ are shown in Fig. 14 as a function of the calcination temperature. Thermal treatments at subsequent temperatures are cumulative. The surface area sharply decreases from room temperature to 300–500 °C, increases at 600 °C, and gradually decreases with further increase in firing temperature. The pore volume shows a small increase between 300 and 500 °C and a sharp jump at higher temperature, its value becoming maximum at 700 °C. Gel treated at higher temperatures shows a sharp reduction in pore volume. Values of both the surface area and the pore volume probably become maximum at ~ 650 °C as shown by the broken lines in Fig. 14. The increase in surface area and pore volume at intermediate temperatures may be ascribed to the decomposition of nitrate and the loss of solvents trapped within the micropores of the dried gel. These results are consistent with the DTA, TGA, and infrared analyses as described above. The rapid reduction in both pore volume and surface area at higher temperatures may be attributed to densification due to sintering.

Scanning electron microscopy of the $10CaO–90SiO_2$ gel calcined to 800 °C at 2 °C min^{-1} followed by isothermal heat treatments at 800 °C for 23 h and at 900 °C for 8 h in air showed the material to be dense. However, pores were present in certain regions of the sample as shown in the scanning electron micrograph (Fig. 15). Similar behaviour has been recently observed by Woignier *et al.* [21] when silica glasses prepared by densification of the aerogels were heated at temperatures above 1200 °C. This porosity is

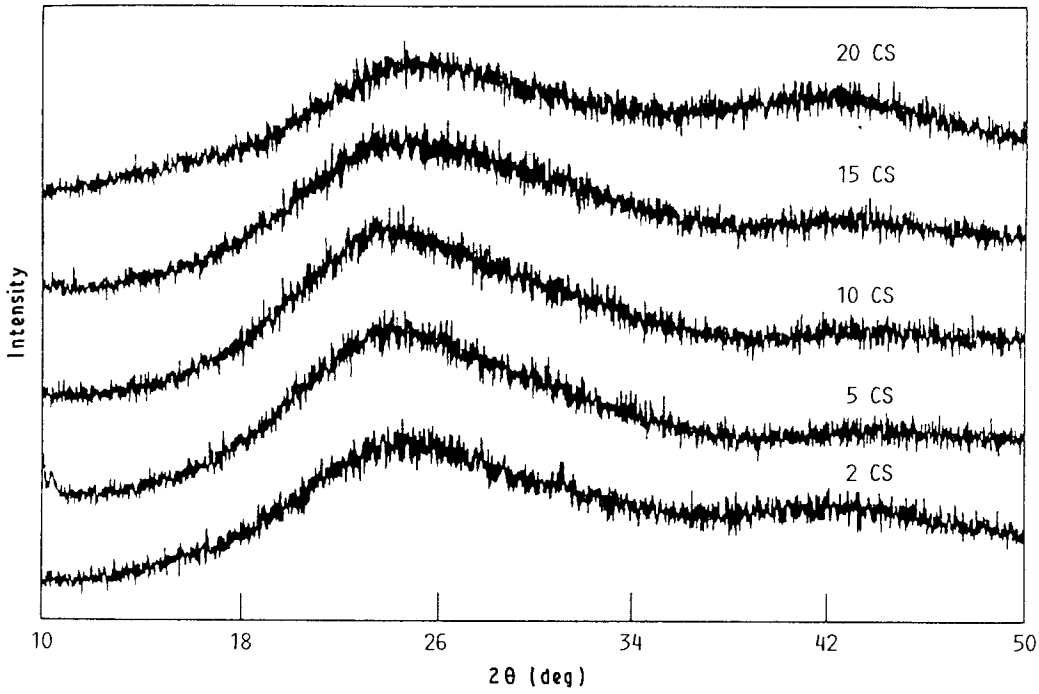

Figure 10 X-ray diffraction spectra of $CaO–SiO_2$ gels of various compositions after drying at 66 °C for 7 days in air.

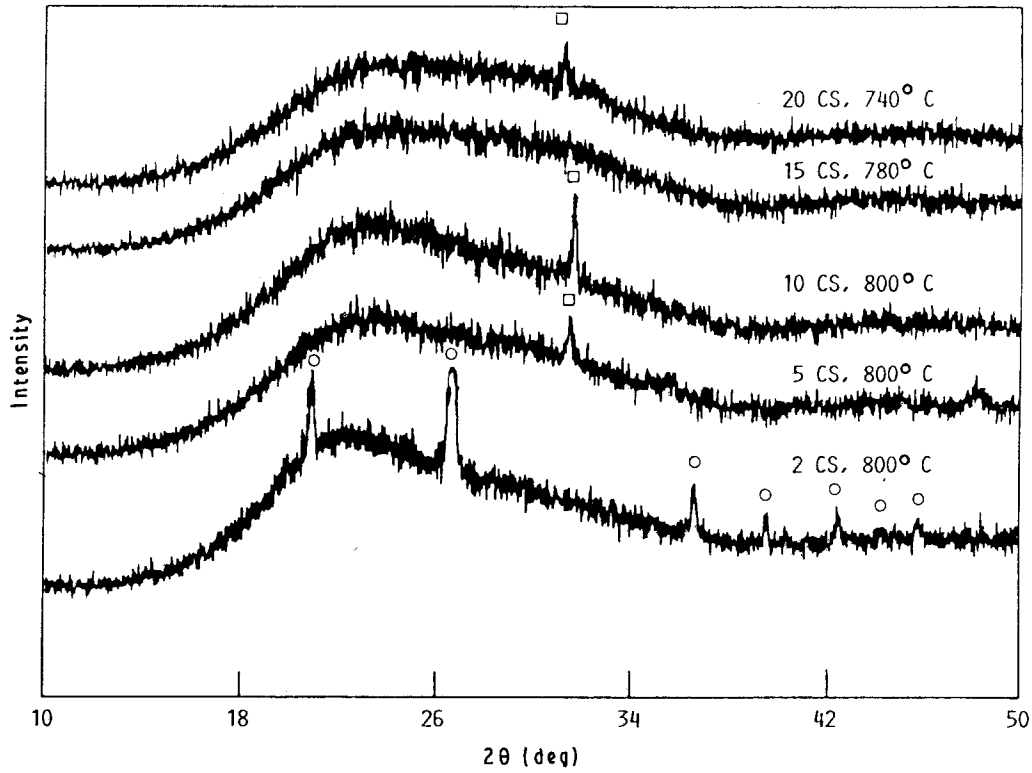

Figure 11 X-ray diffraction patterns of $CaO–SiO_2$ gels of various compositions heated in flowing air up to the temperatures indicated at $\sim 2\,°C\,min^{-1}$ and furnace cooled. (○) α-quartz, (□) holder.

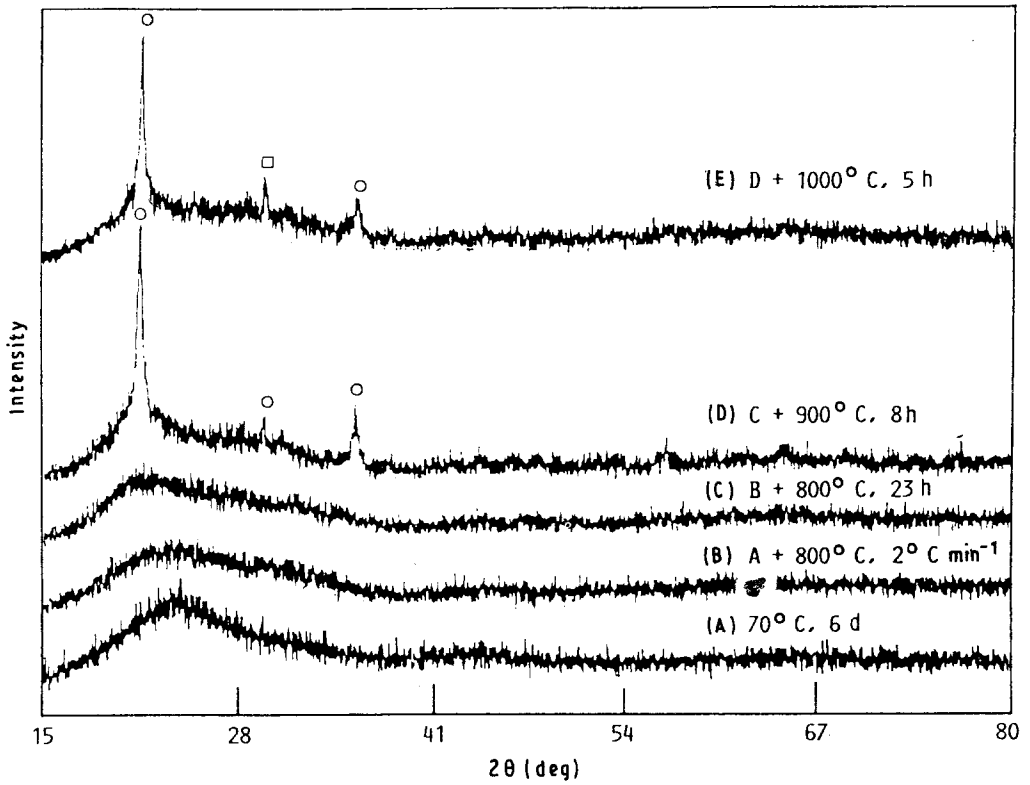

Figure 12 X-ray diffraction spectra of $10CaO–90SiO_2$ (mol %) gel calcined in air at various temperatures. (○) α-cristobalite, (□) wollastonite.

caused by foaming due to the high OH content in the interior of the dense material. During thermal treatment, the surface of the specimen is densified before the interior which makes it difficult to remove the OH species present within the interior pores. The water vapour formed from decomposition of the OH groups becomes trapped in the micropores. At higher temperatures, the increased water vapour pressure in the closed micropores results in bloating.

4. Discussion

Gelation of TEOS occurs in two stages, the hydrolysis and the condensation steps, as represented by the

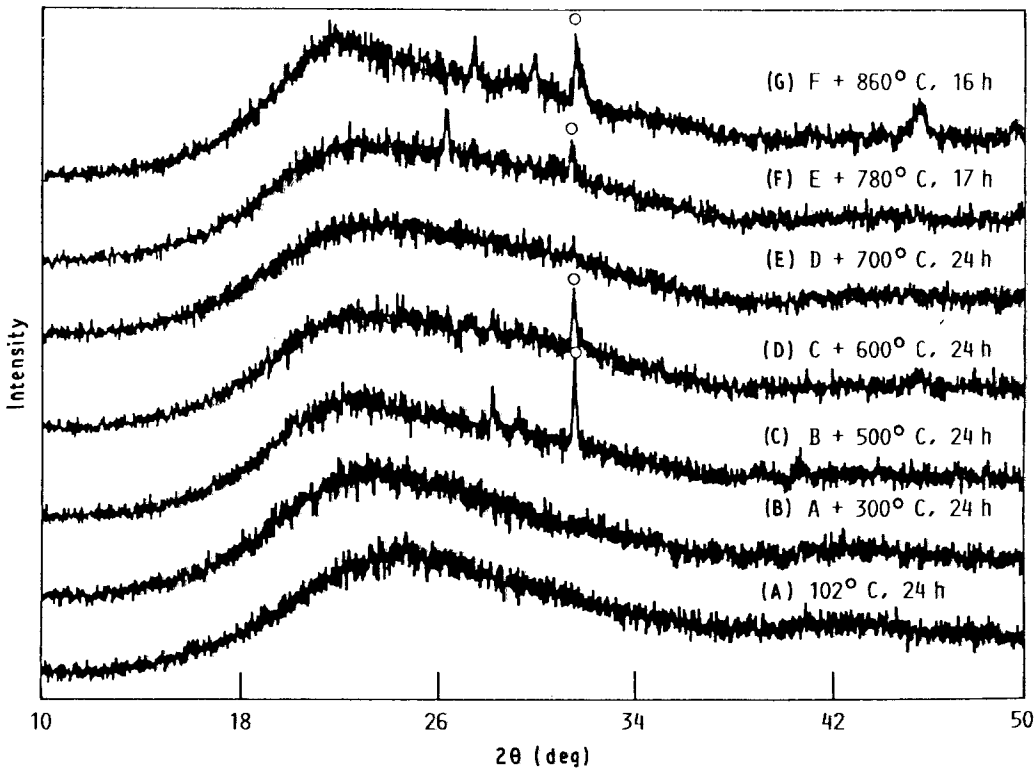

Figure 13 X-ray diffraction patterns of $10CaO–90SiO_2$ (mol %) gel heat treated in air at various temperatures for different times. (○) Holder.

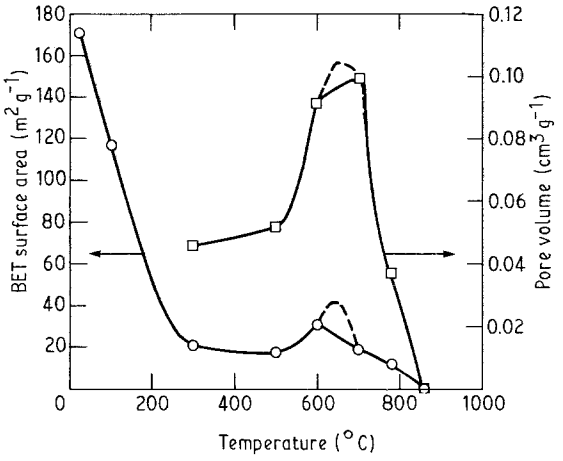

Figure 14 Variations in BET surface area and cumulative pore volume versus calcination temperature of $10CaO–90SiO_2$ (mol %) gel; water:$Si(OC_2H_5)_4$ mole ratio = 4.95; the heat treatments are cumulative at subsequent temperatures. Gel dried under ambient conditions for ~2 months, for 24 h each at 102, 300, 500, 600, and 700 °C, for 17 h at 780 °C, and for 16 h at 860 °C.

following reactions:

$$Si(OEt)_4 + nH_2O \rightarrow Si(OEt)_{4-n}(OH)_n + nEtOH \quad (1)$$

$$-Si-OH + EtO-Si- \rightarrow -Si-O-Si- + EtOH \quad (2a)$$

$$-Si-OH + OH-Si- \rightarrow -Si-O-Si- + H_2O \quad (2b)$$

where Et represents the C_2H_5 group and n varies from 1–4. The condensation process, occurring via dealcoholation (Equation 2a) or dehydration (Equation 2b) steps, results in the formation of –Si–O–Si– bonds.

In the absence of a catalyst, as is the case in the present study, hydrolysis of TEOS is rather slow so that condensation of the partially hydrolysed monomers occurs simultaneously with the hydrolysis step. It is difficult to separate hydrolysis from condensation. However, in the presence of an acid catalyst, hydrolysis is considered to be complete [22] just after the addition of water, as long as a large excess of water is present, and condensation is the rate-controlling process [10]. The rate of hydrolysis is known to increase monotonically [23] as the pH decreases from 7, but the condensation reaction rate shows a local minimum at around pH 2. In this region, hydrolysis may well go to completion before any significant condensation occurs and polymerization will have the normal pattern. Higher water content also promotes hydrolysis and tends to inhibit condensation. It is also known [23] that the time of gelling of silica sols is lowered in the presence of sodium salts at all pH. The presence of sodium salts has little effect on gel time at low pH (~ 1–3) but in the neutral region, the pH of minimum sol stability is increased from ~ 5.5 to 7. The presence of the salts probably helps in lowering the ionic charge on the sol particles. The lowered values of gel times in the presence of Ca^{2+} ions, as observed in the present study, may also be caused by a similar mechanism.

The temperature dependence of the rate of gel formation may be expressed as

$$k = A\exp(-E^*/RT) \quad (3)$$

where k is the reaction rate constant, A the frequency factor, E^* the apparent activation energy, R the gas constant, and T the reaction temperature in Kelvin. The time of gel formation, t_{gel}, may be taken as the average rate of gelation and Equation 3 may be

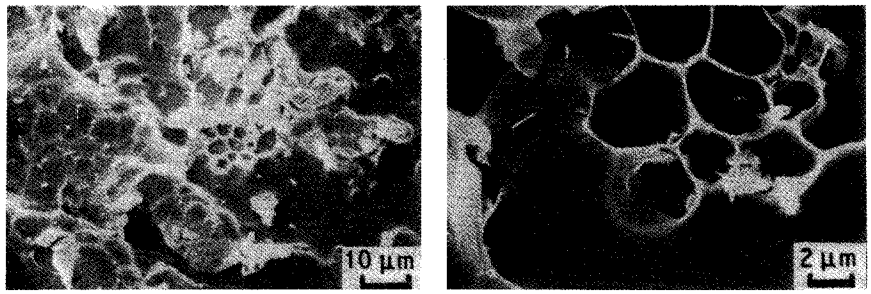

Figure 15 Scanning electron micrographs of the $10CaO–90SiO_2$ (mol %) gel heat treated to 800 °C at 2 °C min^{-1} followed by isothermal heat treatments at 800 °C for 23 h and at 900 °C for 8 h in air.

written as

$$1/t_{gel} = A' \exp(-E^*/RT) \quad (4)$$

Taking the logarithm of Equation 4 gives

$$\log(t_{gel}) = -\log A' + E^*/(2.3026RT) \quad (5)$$

according to which a plot of $\log(t_{gel})$ versus $1/T$ should be linear with a slope of $(E^*/2.3026R)$. The values of E^* and A' can be evaluated from the slope and the intercept, respectively.

Plots of $\log(t_{gel})$ versus $1/T$ for the gelation of $10CaO–90SiO_2$ composition at three water:TEOS mole ratios are presented in Fig. 16. The solid lines in this and the next figure are from linear least-squares fitting of the experimental data to Equation 5. In all cases the value of the correlation coefficient exceeded 0.99. Values of the parameters E^* and A', evaluated from linear least-squares curve fitting of the experimental data, are listed in Table IV. The presence of Ca^{2+} ions or the water:TEOS mole ratio have no appreciable effect on E^*. Similar results in the presence of many other metal ions (Li^+, Na^+, Mg^{2+}, Sr^{2+}) have been reported recently by the present author [9]. However, a sharp increase in gel formation time and the gelation activation energy was observed [9] in the presence of other cations (Al^{3+}, La^{3+}, Y^{3+}) which undergo hydrolysis in the solution.

Fig. 17 shows the plots of $\log(t_{gel})$ versus $1/T$ for three concentrations of Ca^{2+} ions at the same value of $r = 6$. Also shown for comparison is the plot for SiO_2. All the plots are linear indicating applicability of Equation 5. Values of the Arrhenius parameters evaluated from linear least-squares curve fitting of the experimental data are given in Table V. The Ca^{2+} ion concentration has virtually no influence on the value of E^*. The gelation activation energy is probably related [24, 25] to the transport of the condensing species during the polymerization process and not to the Si–O bond energies.

Aelion *et al.* [22] and Vekhov *et al.* [26, 27] reported values of 26.4 and 28.4 kJ mol^{-1}, respectively, for the hydrolysis activation energy of TEOS. Colby *et al.* attributed [24] a value of 19.4 kJ mol^{-1} to the activation energy of hydrolysis rather than polycondensation for the TEOS system at $r = 4$ in the absence of a catalyst. These values are much lower than those obtained in the present work (54.5 kJ mol^{-1}) at $r = 6$ in the absence of a catalyst. Values of 61.1 and 55.2 kJ mol^{-1} have been reported [24, 25] for gelation activation energy of TEOS at r

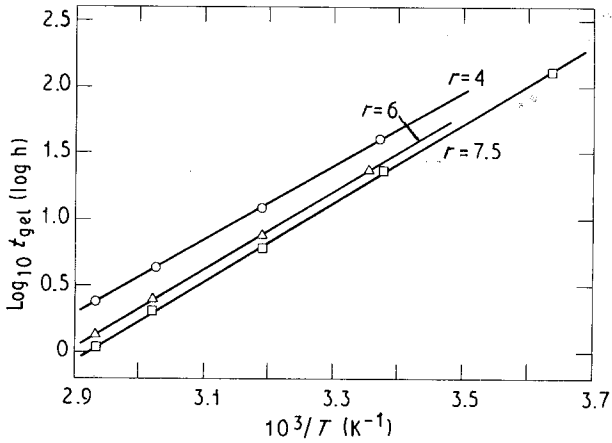

Figure 16 Temperature dependence of gel formation time for $10CaO–90SiO_2$ (mol %) composition at various water:$Si(OC_2H_5)_4$ mole ratios, r.

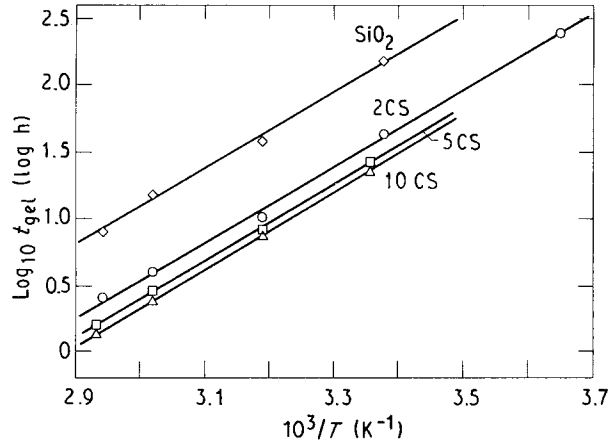

Figure 17 Temperature dependence of gelling time for various $CaO–SiO_2$ compositions; water:$Si(OC_2H_5)_4$ mole ratio = 6.

= 4 in the presence of HF and HCl catalysts, respectively. For the HCl-catalysed TEOS system, Bechtold *et al.* [28, 29] reported values of 40–70 kJ mol^{-1} depending on water concentration.

According to Colby *et al.* [24], if hydrolysis is the rate-determining step, the gelation time should decrease with increase in r even after sufficient water for hydrolysis is present. Also, the activation energy should decrease with increase in r, if the hydrolysis was not complete. For the acid-catalysed TEOS system, Colby *et al.* [24] showed that the gelation time did not decrease with increase in water concentration when enough water was present. But in the absence of sufficient water to complete hydrolysis, the activation

energy systematically decreased when r was increased from 3 to 3.5–4. The higher activation energy at low r was attributed [24] to the steric hindrance offered by the non-hydrolysed alkoxy groups still attached to silicon. For the 10CS system, t_{gel} systematically decreased when r was increased from 4 to 7.5 but the activation energy was more or less independent of the water concentration. This probably indicates that hydrolysis is the rate-determining step and the calculated activation energy is for this process. However, these values are much higher than a value of 19.4 kJ mol^{-1} reported by Colby *et al.* [24] for the hydrolysis activation energy for TEOS at $r = 4$ in the absence of a catalyst.

From XRD, no crystalline phase was detected in the dried gels indicating incorporation of the Ca^{2+} ions into the silica gel network possibly by a cation exchange reaction [30] between the Ca^{2+} ions and the weakly acidic silanol group

$$Ca^{2+} + 2(\text{–Si–OH}) \rightarrow Ca(\text{OSi–})_2 + 2H^+ \quad (6)$$

Probably the Ca^{2+} ions are only loosely bonded in the gel. In acidic solutions, Reaction 6 is reversible [30] and is the sum of the following two reactions

$$\text{–Si–OH} \rightleftharpoons \text{–Si–O}^- + H^+ \quad (7)$$

$$Ca^{2+} + 2(\text{–Si–O}^-) \rightleftharpoons Ca(\text{OSi–})_2 \quad (8)$$

However, crystallization of other metal salts has been reported during drying of various metal silicate gels. Yamane and Kojima [3] observed precipitation of strontium nitrate during the synthesis of $12.7SrO–87.3SiO_2$ (mol %) gels from $Sr(NO_3)_2$ and tetramethoxysilane. Sodium nitrate crystallized out on desiccating $Na_2O–B_2O_3–SiO_2$ gels [5]. Crystallization of $Mg(NO_3)_2 \cdot 6H_2O$ was observed by the present author [1] during drying of $20MgO \cdot 80SiO_2$ (mol %) gels prepared from magnesium nitrate and TEOS.

5. Summary and conclusions

$CaO–SiO_2$ glass compositions having stable liquid–liquid immiscibility have been prepared at low temperatures by the sol–gel method using calcium nitrate and TEOS. Gels containing up to 20 mol % calcium nitrate were clear and transparent. The time of gelation decreased with increase in calcium or water concentration and temperature. The value of E_{gel}, determined from the temperature dependence of the gel time using the Arrhenius equation, was more or less unaffected by the Ca^{2+} as well as the water content. Chemical and structural evolutions in the gels, after various thermal treatments, were followed using TGA, DTA, infrared spectroscopy, X-ray diffraction, surface area and pore size distribution measurements. Glycerol was effective as a drying control agent to form crack-free monolithic gel bodies.

Calcium silicate glass compositions lying within the liquid–liquid immiscibility region, which cannot be prepared by the conventional glass melting method, can be synthesized at low temperatures by the sol–gel process using tetraethoxysilane and calcium nitrate.

Acknowledgements

The technical assistance of Anna Palczer, Ralph Garlick, and Beth Hyatt during the course of this research is very much appreciated.

References

1. N. P. BANSAL, *J. Amer. Ceram. Soc.* **71** (1988) 666.
2. T. HAYASHI and H. SAITO, *J. Mater. Sci.* **15** (1980) 1971.
3. M. YAMANE and T. KOJIMA, *J. Non-Cryst. Solids* **44** (1981) 181.
4. M. V. VILLEGAS and J. M. FERNANDEZ NAVARRO, *J. Mater. Sci.* **23** (1988) 2142.
5. S. P. MUKHERJEE, in "Materials Processing in the Reduced Gravity Environment of Space", edited by G. E. Rindone (North-Holland, New York, 1982) pp. 321–30.
6. F. PANCRAZI, J. PHALIPPOU, F. SORRENTINO and J. ZARZYCKI, *J. Non-Cryst. Solids* **63** (1984) 81.
7. W. K. TREDWAY and S. H. RISBUD, *ibid.* **100** (1988) 278.
8. H. D. LUTH, *Z. Anorg. Allg. Chem.* **353** (1967) 207.
9. N. P. BANSAL, *J. Amer. Ceram. Soc.* **73** (1990) 2647.
10. S. SAKKA, in "Treatise on Materials Science and Technology", Vol. 22, "Glass III", edited by M. Tomozawa and R. H. Doremus (Academic Press, New York, 1982) pp. 129–67.
11. I. MATSUYAMA, K. SUSA, S. SATOH and T. SUGANUMA, *Amer. Ceram. Soc. Bull.* **63** (1984) 1408.
12. M. DECOTTIGNIES, J. PHALIPPOU and J. ZARZYCKI, *J. Mater. Sci.* **13** (1978) 2605.
13. G. H. SIGEL, in "Treatise on Materials Science and Technology", Vol. 12, "Glass I; Interaction with Electromagnetic Radiation", edited by M. Tomozawa and R. H. Doremus (Academic Press, New York, 1977) pp. 5–89.
14. J. WONG and C. A. ANGELL, *Appl. Spectrosc. Rev.* **4** (1971) 155.
15. I. SIMON, in "Modern Aspects of the Vitreous State", Vol. 1, edited by J. D. Mackenzie (Butterworths, London, 1960) pp. 120–51.
16. R. HANNA, *J. Amer. Ceram. Soc.* **48** (1965) 595.
17. I. NAKAGAWA and J. L. WALTER, *J. Chem. Phys.* **51** (1969) 1389.
18. M. L. HAIR, *J. Non-Cryst. Solids* **19** (1975) 299.
19. K. KAMIYA, S. SAKKA and M. MIZUTANI, *Yogyo Kyokaishi* **86** (1978) 552.
20. A. K. VARSHNEYA and N. SUH, *J. Amer. Ceram. Soc.* **70** (1987) C-21.
21. T. WOIGNIER, J. PHALIPPOU and M. PRASSAS, *J. Mater. Sci.* **25** (1990) 3118.
22. R. AELION, A. LOEBEL and F. EIRICH, *J. Amer. Chem. Soc.* **72** (1950) 5705.
23. R. K. ILER, 'The Chemistry of Silica: Solubility, Polymerization, Colloid and Surface Properties, and Biochemistry" (Wiley Interscience, New York, 1979).
24. M. W. COLBY, A. OSAKA and J. D. MACKENZIE, *J. Non-Cryst. Solids* **99** (1988) 129.
25. *Idem., ibid.* **82** (1986) 37.
26. V. A. VEKHOV, E. P. DUDNIK and K. G. MARIN, *Russ. J. Inorg. Chem.* **9** (1964) 294.
27. V. A. VEKHOV, E. P. DUDNIK and E. I. RUMYANTSEVA, *ibid.* **10** (1965) 1281.
28. M. F. BECHTOLD, W. MAHLER and R. A. SCHUNN, *J. Polymer Sci. Polym. Chem. Ed.* **18** (1980) 2823.
29. M. F. BECHTOLD, R. D. VEST and L. PLAMBECK Jr, *J. Amer Chem. Soc.* **90** (1968) 4590.
30. D. L. DUGGER, J. H. STANTON, B. N. IRBY, B. L. McCONNELL, W. W. CUMMINGS and R. W. MAATMAN, *J. Phys. Chem.* **68** (1964) 757.

Received 29 January
and accepted 28 May 1991